2.9

ATMOSPHERIC RESPONSE TO SEA-SURFACE TEMPERATURE VARIABILITY

D. Vickers* and L. Mahrt
Oregon State University, Corvallis, OR, USA

1. INTRODUCTION

Stronger turbulent mixing and potentially larger fluxes are associated with flow over warmer water due to enhanced buoyancy generation of turbulence, or in the case of stratified flow, decreased buoyancy suppression of shear-generated turbulence. In addition to the effect of enhanced mixing, the fluxes of heat and moisture are directly related to SST through the air-sea temperature and air-sea humidity differences in the bulk flux formula.

Traditional arguments predict a stronger flux response to small-scale surface features in stable flow due to the decreased length scale of the eddies responsible for the flux. In contrast, footprint theory predicts a larger area of influence, and thus a reduced correlation with the local surface in stable flow. Strongly stratified flow may become partially decoupled from the surface, reducing the response (Mahrt et al., 2001). One complication with addressing these ideas with measurements is that random flux sampling errors are more severe in stable conditions.

In this study we use aircraft eddy correlation flux and SST measurements collected over cold and warm pools in the coastal region of the Atlantic Ocean to examine the turbulent flux response to changes in SST. Here we focus on the heat flux response. In the oral presentation we examine the height-dependence of the mean wind response to an increase in SST using a case study.

2. DATA

We use data collected by the NOAA LongEZ (N3R) aircraft during the pilot program of the CBLAST experiment conducted over the Atlantic Ocean south of Martha's Vineyard Island, MA, USA, during July and August of 2001. Eddy correlation fluxes were calculated using low altitude (10 *m*) flight segments where aircraft altitude, roll, pitch and heading fluctuations remained within prescribed limits and where the track was either primarily into or following the mean wind, enabling an estimate of the SST in the flux footprint, but significantly reducing the size of the data set. With these restrictions, the set includes 74 flight segments on 9 different flight days which include 3 days with unstable conditions with cold dry air outbreaks from the north and 6 days of stable conditions with warm moist air advected from the southwest. All references to temperature (T) refer to the local potential temperature.

Using too small a window size to compute the perturbations can lead to systematic flux loss and underestimation of the flux, while using too large a window can include poorly sampled nonturbulent motions especially in stable conditions (Vickers and Mahrt, 2003). In extreme weak turbulence, a flux calculation may not be well posed due to strong scale-dependence. The sensitivity of the calculated heat flux to the window size τ used to define the perturbations is briefly explored below. Products of perturbations, e.g. $w'\theta'$, are averaged over a range of scales referred to as the flux averaging scale (λ).

The upwind distance to the surface footprint of the flux can be approximated as zU/σ_w based on simple scaling arguments where the vertical transfer is proportional to the standard deviation of the vertical velocity fluctuations (σ_w) and horizontal transfer is equal to the mean wind speed (U). Footprints calculated using the measurements range from 100 to 1000 m depending on the particular flight segment. This simple estimate may breakdown when the strength of the mixing or the mean wind speed changes rapidly with height. Calculation of the fluxes for a sequence of upwind spatial lags with respect to the SST showed that on average the correlation between SST and the heat flux decreased slowly with increasing lag. The 2-*km* lag correlation is larger than the zero lag correlation in a few cases with weak vertical mixing, for example in the 30 to 35 *km* region of Figure 2a at the sharp SST front.

The stable boundary layer depth ranged from 30 to 200 *m* depending on the day and region based on vertical profiles from aircraft slant soundings (Vickers and Mahrt, 2004). In the shallowest stable boundary layer cases, the 10-*m* flux measurement level could be above the surface layer.

3. HEAT FLUX RESPONSE

The correlation between the heat flux and a bulk model type prediction of the heat flux using mean variables is significant for these data (Figure 1). The correlation in-

* *corresponding author address:* Dean Vickers, College of Oceanic and Atmospheric Sciences, Oregon State University, Corvallis, OR; *email*: vickers@coas.oregonstate.edu

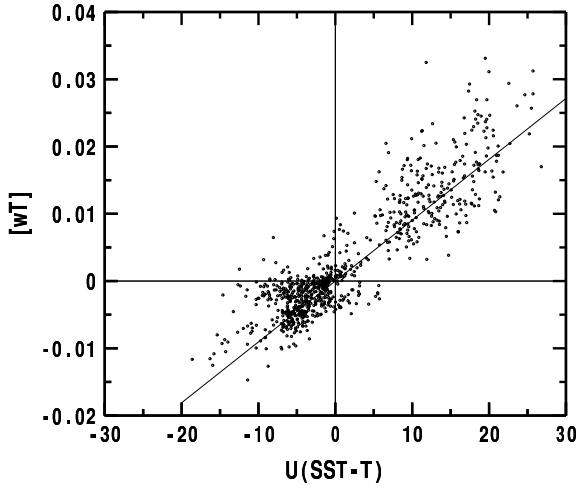

Figure 1: $\tau = \lambda = 2$-*km* averaged heat flux versus the mean wind speed times the stratification for all days combined. The slope of the linear regression line (C_h) is 0.9 $x10^{-3}$. The fractional variance explained is 0.81.

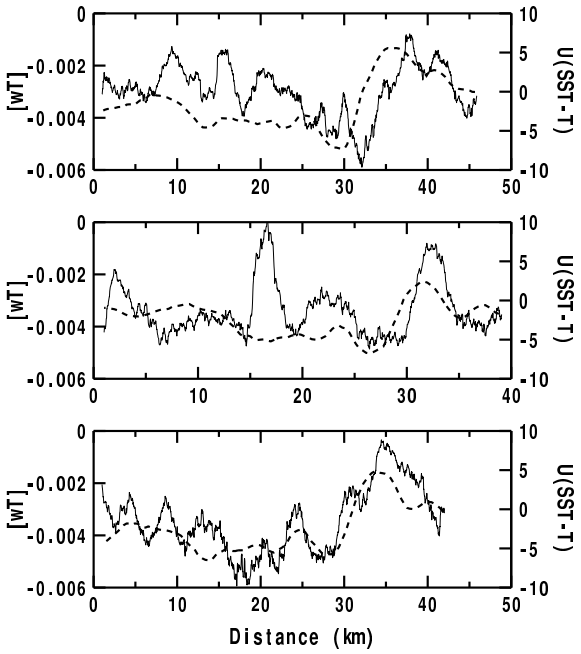

Figure 2: Spatial variation of the heat flux (solid line) and $U(SST - T)$ for 3 passes over the same track on 23 July in weakly stable flow. $\tau = \lambda = 2$ *km*. The mean flow is left to right.

creases slightly as the flux averaging window size λ increases from 2 to 10 *km*. Using $\tau = 100$ *m* or 500 *m* in stable conditions to better exclude poorly sampled non-turbulent motions removes some counter-gradient heat fluxes and increases the overall correlation slightly, although the magnitude of the downward heat flux is significantly reduced using $\tau = 100$ *m* in some cases. Increasing τ to 4 *km* for unstable conditions to capture even larger eddies has small impact on the calculated heat flux for these data.

Replacing the observed variable 2-*km* mean wind speed with a constant reduces the fractional variance explained (Figure 1) from 0.81 to 0.76, indicating that the mean wind speed influence is secondary to the stratification for the heat flux. The slope of the regression line forced through the origin (Figure 1) is an estimate of the exchange coefficient for heat.

There is considerable scatter for individual flight segments, especially for tracks with weak downward heat fluxes (Figure 2). The heat flux is apparently sometimes modulated by processes unrelated to the local mean wind speed or stratification, for example where the heat flux collapses to zero in the 15 to 20 *km* region of Figure 2b. The between-pass variability of the heat flux is large, indicating that more than 3 passes would be required to reduce random sampling errors to an acceptable level in this example. Therefore, much of the scatter in Figure 1 is due to random flux sampling errors. The correlation between SST features and the heat flux tends to be larger for unstable conditions (Figure 3) although large unexplained variability in the heat flux remains.

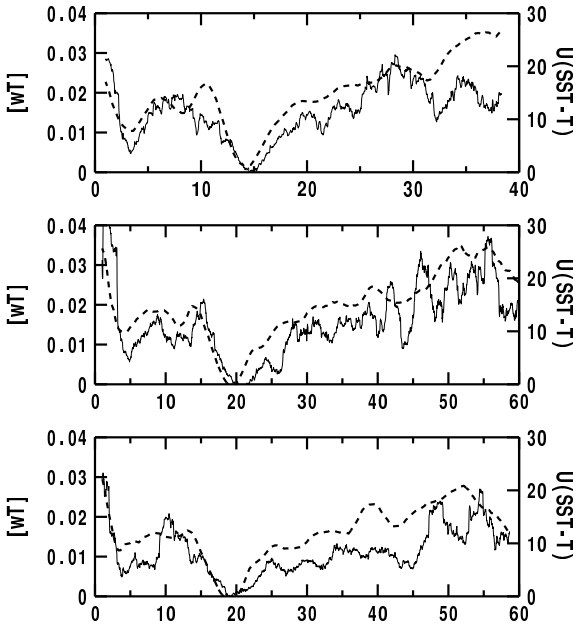

Figure 3: Same as Figure 2 except for 3 passes on 27 July in unstable flow.

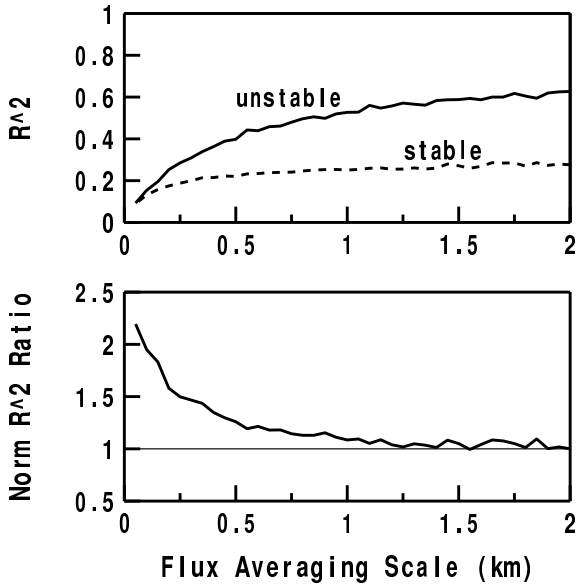

Figure 4: Dependence of R^2 on flux averaging scale for correlation between the heat flux and $U(SST-T)$ for unstable and stable conditions (top), and the normalized R^2 for stable conditions divided by the normalized R^2 for unstable conditions (bottom). $\tau = 500$ *m* for stable and 4 *km* for unstable conditions.

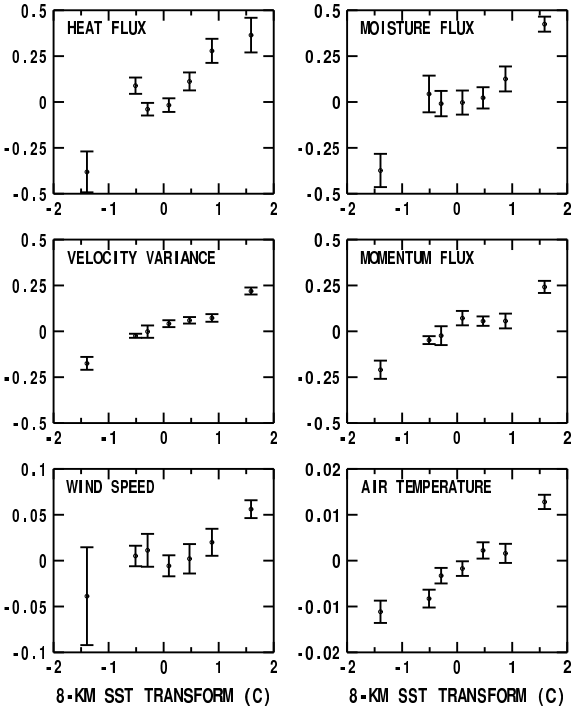

Figure 5: Mean and standard error of the relative change (downwind minus upwind divided by the mean) in the fluxes and mean fields as a function of the SST Haar transform (*C*). Data has been bin-averaged such that each bin contains an equal number of samples. $\tau = 2$ *km*, $\lambda = 4$ *km*.

4. SCALE DEPENDENCE

The correlation between the heat flux and $U(SST-T)$ increases rapidly at small spatial scales for unstable flows and then begins to level off for flux averaging scales between 1 and 2 *km* (Figure 4a). It then remains nearly constant out to the 20 *km* scale. The correlation is larger for unstable conditions presumably due to larger random flux sampling problems in stable conditions. In addition, the 10 *m* measurement level may be too high in the shallowest stable boundary layer cases.

When R^2 is normalized by it's value at large flux averaging scales (here 2-*km*), the ratio of the variance explained in stable conditions to that in unstable conditions increases with decreasing scale (Figure 4b). This is in agreement with traditional arguments that the larger scale eddies associated with unstable conditions are less influenced by small-scale surface features. The characteristic scale of the eddies as measured by the peak of the vertical velocity spectra for weakly stable conditions (Figure 2) is an order of magnitude smaller than for unstable conditions (Figure 3). The normalized R^2 ratio is smaller than shown in Figure 4b when computing the perturbations using a fixed $\tau = 2$ *km* for all conditions..

5. AMPLITUDE OF RESPONSE

Discontinuities in SST are identified using the Haar transform, which calculates the difference in SST over two 4-*km* half window means. A large positive (negative) value of the transform indicates an increase (decrease) in SST in the downwind direction which is coherent on the scale of the window (8-*km*). The structure surrounding SST fronts is composited based on the value of the transform to examine the response of the fluxes and mean fields to the amplitude of the SST fronts. The fluxes and vertical velocity variance respond strongly when the transform exceeds 1 *C*, equivalent to an SST gradient of 0.25 Ckm^{-1} (Figure 5). When the SST gradient is less than this, the response is of questionable significance. The magnitude of the relative flux response is similar for flow over cold-to-warm and warm-to-cold SST discontinuities.

There are small yet systematic changes in the mean wind speed and air temperature across the discontinuities (Figure 5). The 10-*m* mean wind speed increases an average of 6% with small scatter for all SST increases between 1 and 2 *C*. There is large scatter in the mean wind speed response to a decrease in SST. As the flow moves

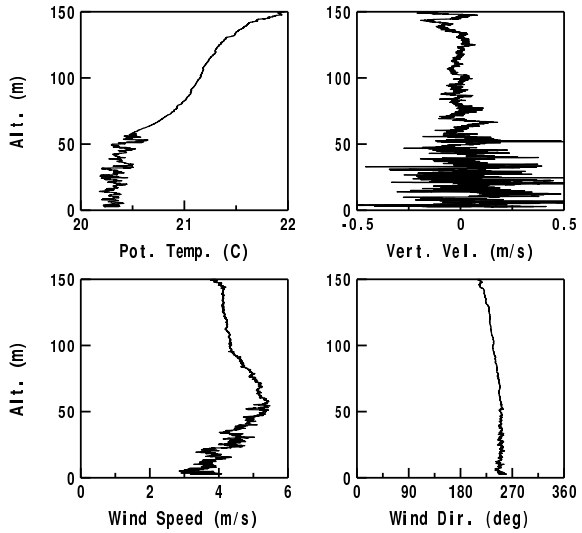

Figure 6: Example shallow stable boundary-layer structure from an aircraft slant sounding on 1 August.

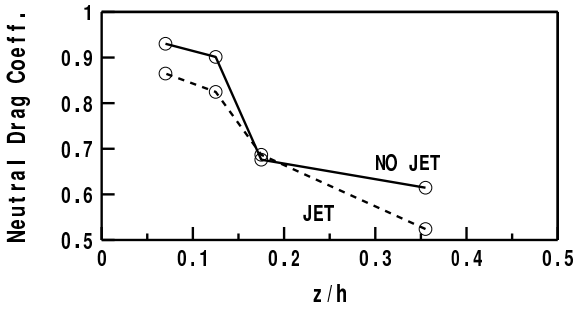

Figure 7: Demonstration of failure of Monin-Obukov similarity theory applied to 10-*m* measurements in stable flow due to a dependence of the neutral drag coefficient on stable boundary layer depth *h*. Values are bin-averages.

from colder water to over warmer water, the mean flow at 10 *m* warms, moistens, accelerates and becomes more turbulent. The opposite is true for flow from warm to cold water.

6. SHALLOW BOUNDARY LAYERS

In stable boundary layers, the top of a surface-based turbulent layer, a temperature inversion and a low-level wind jet were often colocated (Figure 6). Monin-Obukov similarity theory applied to the 10-m momentum flux measurements fails in the most shallow stable boundary layer periods apparently due to the importance of z/h and the implied vertical flux divergence between the surface and 10 *m* (Figure 7). The departure is slightly more severe when a low-level jet is present at the top of the boundary layer, as also observed by Smedman et. al. (1995). The low-level jet is thought to suppress large scale eddies, although the mechanism responsible is not well understood.

7. ACKNOWLEDGMENTS

This material is based upon work supported by Grant N00014-01-1-0084 from the Marine Meteorology Program of the Office of Naval Research.

REFERENCES

Mahrt,L., D.Vickers, J.Sun, T.L.Crawford, G.Crescenti, and P.Frederickson, 2001, Surface stress in offshore flow and quasi-frictional decoupling. *J. Geophys. Res.*, **106**, 20629-20639.

Smedman,A-S., H.Bergström, and U.Högström. 1995, Spectra, variances and length scales in a marine stable boundary layer dominated by a low level jet. *Boundary-Layer Meteorol.*, **76**, 211-232.

Vickers,D., and L.Mahrt, 2003, The cospectral gap and turbulent flux calculations. *J. Atm. Oc. Tech.*, **20**, 660-672.

Vickers,D., and L.Mahrt, 2004, Evaluating formulations of stable boundary-layer height. *J. Appl. Meteor.*, in press.